

Research Paper

Magnetoliposomes Loaded with Poly-Unsaturated Fatty Acids as Novel Theranostic Anti-Inflammatory Formulations

Daniel Calle¹, Viviana Negri^{1,2}, Paloma Ballesteros² and Sebastián Cerdán¹✉

1. Instituto de Investigaciones Biomédicas “Alberto Sols” CSIC/UAM, c/ Arturo Duperier 4, Madrid 28029, Spain.
2. Laboratorio de Síntesis Orgánica e Imagen Molecular por Resonancia Magnética, Facultad de Ciencias, UNED, Unidad Asociada al CSIC, c/ Paseo Senda del Rey 9, Madrid 28040, Spain.

✉ Corresponding author: Prof. Sebastian Cerdan, Instituto de Investigaciones Biomédicas “Alberto Sols” CSIC/UAM c/ Arturo Duperier 4, Madrid 28029, Spain. Phone: 0034-91-585-4444 Fax: 0034-91-585-4401 Email: scerdan@iib.uam.es.

© 2015 Ivyspring International Publisher. Reproduction is permitted for personal, noncommercial use, provided that the article is in whole, unmodified, and properly cited. Please see <http://ivyspring.com/terms> for terms and conditions.

Received: 2014.07.09; Accepted: 2014.12.18; Published: 2015.02.15

Abstract

We describe the preparation, physico-chemical characterization and anti-inflammatory properties of liposomes containing the superparamagnetic nanoparticle Nanotex, the fluorescent dye Rhodamine-100 and omega-3 polyunsaturated fatty acid ethyl ester (ω -3 PUFA-EE), as theranostic anti-inflammatory agents. Liposomes were prepared after drying chloroform suspensions of egg phosphatidylcholine, hydration of the lipid film with aqueous phases containing or not Nanotex, Rhodamine-100 dye or ω -3 PUFA-EE, and eleven extrusion steps through nanometric membrane filters. This resulted in uniform preparations of liposomes of approximately 200 nm diameter. Extraliposomal contents were removed from the preparation by gel filtration chromatography. High Resolution Magic Angle Spinning ¹H NMR Spectroscopy of the liposomal preparations containing ω -3 PUFA-EE revealed well resolved ¹H resonances from highly mobile ω -3 PUFA-EE, suggesting the formation of very small (ca. 10 nm) ω -3 PUFA-EE nanogoticles, tumbling fast in the NMR timescale. Chloroform extraction of the liposomal preparations revealed additionally the incorporation of ω -3 PUFA-EE within the membrane domain. Water diffusion weighted spectra, indicated that the goticles of ω -3 PUFA-EE or its insertion in the membrane did not affect the average translational diffusion coefficient of water, suggesting an intraliposomal localization, that was confirmed by ultrafiltration. The therapeutic efficacy of these preparations was tested in two different models of inflammatory disease as inflammatory colitis or the inflammatory component associated to glioma development. Results indicate that the magnetoliposomes loaded with ω -3 PUFA-EE allowed MRI visualization in vivo and improved the outcome of inflammatory disease in both animal models, decreasing significantly colonic inflammation and delaying, or even reversing, glioma development. Together, our results indicate that magnetoliposomes loaded with ω -3 PUFA-EE may become useful anti-inflammatory agents for image guided drug delivery.

Key words: Magnetoliposomes, ω -3 poly-unsaturated fatty acid ethyl ester, Superparamagnetic nanoparticle, MRI, Image guided drug delivery.

Introduction

Inflammatory lesions are associated to the most prevalent and morbid pathologies in developed countries including atherosclerosis [1, 2], neuro-

degeneration [3, 4] diabetes or obesity [5, 6] and cancer [7-9], among others. Decreases in the inflammatory phenotype are known to reduce disease progres-

sion and improve patient's quality of life, as well as to enhance recovery [7, 9]. With this aim, a variety of anti-inflammatory drugs have been proposed as adjuvant therapies for the different diseases, including mainly steroidal or non-steroidal treatments [10-12]. However, anti-inflammatory therapies demand the use of relatively large doses of the free drugs and inevitably end up developing, a collection of adverse secondary effects that preclude continuation of the treatment [13, 14]. On these grounds, methods to improve the efficiency of anti-inflammatory drug delivery to the lesion, decreasing the dose and increasing its selectivity and efficacy, entail considerable importance in a wide spectrum of diseases.

Liposomes have been proposed previously as novel nanotechnology formulations to improve drug delivery to a variety of inflammatory diseases [15-17]. Targeting of the inflammatory region may be achieved using, either active or passive approaches. Active targeting involves the use vectorial reagents embedded in the liposomal membrane that recognize epitopes of the target lesion [18]. Passive targeting refers to the passive accumulation of the liposomes in the inflamed regions because of the Enhanced Permeability Retention (EPR), an effect derived from their relatively increased capillary permeability and limited clearance [19]. In both targeting strategies, it becomes difficult to visualize non-invasively if the liposomal preparation has arrived to the target tissue and many times, only indirect measurements of the inflammation size or volume provide an index of the anti-inflammatory effect. It would become then very useful, to be able to locate directly and non-invasively the presence of the drug loaded liposomes in the lesion. Liposomes are optimal structures for this purpose, since they can be prepared to contain in their lumen, in addition to the anti-inflammatory drug, a variety of imaging probes including radioactive, fluorescent or superparamagnetic agents, among others [20-22]. The liposomal lumen can be loaded with water-soluble drugs, maintained in solution in the lumen, or lipid-soluble drugs, thought to incorporate spontaneously in the bilayer membrane [23, 24]. This approach is known as image guided drug delivery, representing currently a powerful strategy to diagnose and treat inflammatory diseases [25-28].

Important anti-inflammatory effects have been reported using preparations of omega-3 fatty acids [29-35], a kind of long chain polyunsaturated fatty acids (PUFAs) mainly present in fish oils and used as dietary supplement. Omega-3 PUFAs allow prolonged anti-inflammatory treatments without the appearance of the deleterious secondary effects of alternative steroidal or non-steroidal drugs [14, 36], operating simultaneously on a variety of targets of the

inflammatory cascade.

In this work we report on a successful protocol to encapsulate ω -3 PUFA [37] containing in addition, either or both, the novel Nanotex superparamagnetic nanoparticle [38] or the Rhodamine-100 dye, thus allowing in vivo monitorization using magnetic resonance imaging or fluorescence. These advanced theranostic preparations maintain completely the therapeutic potential of free ω -3 PUFA, potentiated additionally with highly versatile multimodal imaging capabilities. We demonstrate here the anti-inflammatory effects of these preparations *in vivo*, in animal models of colonic and oncologic inflammation.

Materials and Methods

Preparation of Nanotex

Nanotex is a superparamagnetic nanoparticle containing a magnetite (Fe_3O_4) core with poly(acrylic acid) coating. Magnetite (Fe_3O_4) nanoparticles were prepared by the co-precipitation of Fe^{3+} and Fe^{2+} ions (molar ratio 2:1) at 25 °C and a concentration of 0.3 M iron ions with ammonia solution (29.6%) at pH 10 in an inert atmosphere, followed by hydrothermal treatment at 80 °C for 30 min. For the binding of poly(acrylic acid) (PAA), 100 mg of Fe_3O_4 nanoparticles were first mixed with 2 mL of buffer A (0.003 M phosphate, pH 6) and 0.5 mL of carbodiimide solution (0.025 g/mL in buffer A). After being sonicated for 10 min, 2.5 mL of PAA solution (60 mg/mL in buffer A) was added and the reaction mixture was sonicated for another 30 min. Finally, the PAA-coated Fe_3O_4 nanoparticles were recovered magnetically, washed with water twice and dialyzed against a buffer saline solution. Nanotex preparations were highly water soluble, stable for several months, and depicted uniform diameters smaller than 15 nm [38].

Preparation and characterization of liposomes

Lipid film hydration and extrusion method

Liposomes were prepared essentially using the film hydration method [17, 39, 40]. Briefly, 20 mg (26 μmol) of L- α -phosphatidylcholine (PtdCho, Avanti Polar Lipids Inc. 840051P, Alabaster, Alabama, USA) were dissolved in 2 mL of chloroform (Merck, Darmstadt, DE K36897545). The solution was placed in a round bottom flask and subjected to rotary evaporation (Heindolph Instruments, Schwabach, DE) for sixty minutes (280 rpm, 474 mBar, 40 °C). The lipid film formed after chloroform evaporation was further rotated under the same conditions to remove chloroform traces. Then, the dried lecithin film was rehydrated with 5 mL of water (containing or not the active principle and imaging probes) and rotated 60 minutes at atmospheric pressure and 50 °C. This

process generates a heterogeneous suspension of liposomes of different sizes containing or not the active principles and imaging probes in their lumen or outside as delivered with the hydration buffer. To homogenize the size distribution, the liposomal suspension was extruded eleven times (Northen Lipids, Burnaby, CA) under nitrogen pressure through a 200 nm membrane (Whatman, GE Healthcare, Fairfield, Connecticut, US) maintaining the extrusor temperature at 50 °C. The resulting suspension containing homogenous liposomes, loaded or not with the selected imaging agent and ω -3 PUFA ethyl ester (ω -3 PUFA-EE), was stored at 4 °C until further utilization.

Figure 1A provides a schematic description of the process.

We prepared liposomes encapsulating either suspensions of (i) buffer alone, (ii) Nanotex superparamagnetic nanoparticle (0.5 mg Fe/mL, Solutex S.L., Alcobendas, ES) as MRI detectable probe, (iii) Nanotex and ω -3 PUFA-EE (0.1% v/v final volume, 0.75 mM, 95% w/v eicosapentanoic acid ethyl ester, Solutex S.L., Alcobendas, ES) as theranostic anti-inflammatory agents detectable by MRI, or (iv) Nanotex with Rhodamine-100 chloride (10 mg/mL Sigma Aldrich, Barcelona, ES) as a novel hybrid imaging agent detectable by MRI and fluorescence.

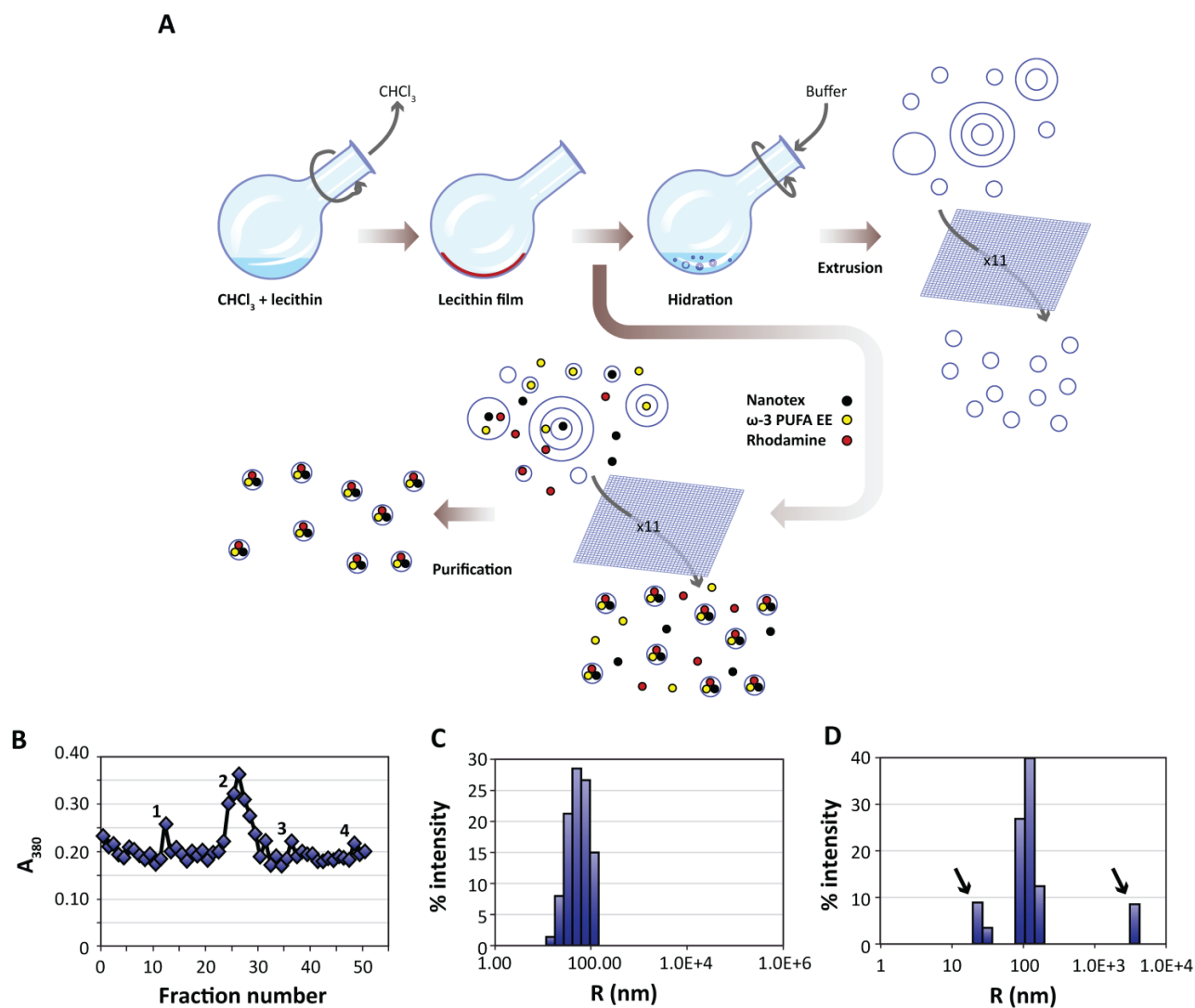


Figure 1. Preparation and characterization of liposomes. A: Liposomes are prepared from egg yolk lecithin, containing or not ω -3 PUFA-EE, Nanotex or Rhodamine-100 by the film hydration method [39]. A solution of chloroform and lecithin is rotated under vacuum to remove chloroform, depositing a thin lecithin film covering the round bottom flask. Hydration of this film with aqueous buffer results liposomes of heterogeneous sizes and different numbers of layers. Nanotex (black circles), ω -3 PUFA-EE (yellow circles) or Rhodamine-100 (red circles) may be added to the buffer, resulting in their intraluminal encapsulation. Some residual Nanotex, ω -3 PUFA-EE or Rhodamine-100 may remain in the extraliposomal space. Repeated extrusions (x11) result in crude homogeneous suspensions of liposomes loaded or not with added components in their lumen, but present also in the extraliposomal space. These may be removed later after a purification process, normally based in size exclusion chromatography (Sephadex G50) or centrifugal ultrafiltration through filters of controlled pore size. B: Absorption (turbidity) peaks at 380 nm from the column fractions loaded with a sample of liposomes with Nanotex and ω -3 PUFA-EE. Note that the elution profile presents an initial peak 1 corresponding to large Nanotex particle aggregates not encapsulated in the liposomes, followed by the most prominent peak 2 derived from liposomes containing PUFA-EE goticules and Nanotex, and extraliposomal free Nanotex particles (peak 3) or PUFA-EE goticules (peak 4). Representative DLS of a suspension of empty liposomes (C) and a suspension of liposomes loaded with ω -3 PUFA-EE (D). Black arrows indicate the size of smaller or larger aggregates of free ω -3 PUFA-EE.

Centrifugal Ultrafiltration

The ultrafiltration method separates the crude liposomal preparation in two fractions, the sediment containing the liposomes, and the ultrafiltrate containing mainly the extraliposomal medium. This is achieved by forcing the crude liposomal preparation to pass through a filter of controlled pore size, under centrifugal acceleration. For this purpose, we used molecular size filters with a pass of 300 KDa (Vivaspin 6, MWCO 300 KDa, Vivaproducts, Littleton, MA, US). The centrifuge used was J-6B (Beckman Coulter, L'Hospitalet de Llobregat, ES) with centrifugation conditions of 2891 G (3900 rpm, 20 °C, 1 hour). After the centrifugation, the absorption spectra (200 - 600 nm) of the sediment and the ultrafiltrate was obtained to determine the presence of PUFA-EE goticules using multiwall plates in a vertical spectrofluorometer (Synergy, Biotek, Winooski, VT, US).

Size exclusion chromatography

Size exclusion chromatography separates the components of a heterogeneous sample according to their size or molecular weight. Those components larger than the pores of the matrix (Sephadex G-50, Sigma-Aldrich, Alcobendas, ES) are excluded from the exchange and proceed faster to the chromatographic front, while those components with smaller size than the matrix pore are temporally retained, with longer elution times for the smaller molecules [39].

The column dimensions were 1.8 x13 cm. Two grams of Sephadex G50 (swell capacity 1 g/9 mL) were hydrated with 40 mL of H₂O Milli-Q (4 °C, 16 hours). After Sephadex hydration, the column was charged and compressed with H₂O Milli-Q (250 mL), stabilizing the flux to 0.3 mL/min. Then, the Sephadex column was presaturated with an empty liposomes preparation to minimize non selective adsorption. Then, 300 µL of the crude liposomal preparation were added to column head and run (0.3 mL/min) with 50 mL of H₂O Milli-Q. Fractions of the eluate were collected automatically (400 µL/90 sec, Biorad 210, BioRad Laboratories, Madrid, ES) and analyzed spectrophotometrically on a vertical plate reader (Synergy, BioTek, VT, US).

Figure 1B shows a representative elution profile from the gel filtration chromatography of a crude preparation of liposomes containing Nanotex and ω-3 PUFA-EE as monitored by measurements of absorbance (turbidity) at 380 nm. The first peak observed (peak 1), co-eluting with the solvent front, corresponds to large aggregates of extraliposomal Nanotex, since it is observed also when running liposome-free Nanotex preparations. The second peak (peak 2) corresponds to liposomes loaded with ω-3

PUFA-EE and Nanotex. Finally, the two peaks eluting later, correspond to small extraliposomal free individual Nanotex particles (peak 3) and external goticules of ω-3 PUFA-EE (peak 4) not entrapped within the liposome, since both co-elute with the corresponding standards, respectively. The comparison of the absorbance (turbidity) measurements between the crude preparation and the purified liposomal fractions lead us to the conclusion that liposomes encapsulate approximately 30% of the added ω-3 PUFA-EE or close to 100% of the added Nanotex.

Dynamic Light Scattering

The size of liposomes (Figure 1C, 1D) was measured by Dynamic Light Scattering (DLS, DynaPro MS/X Wyatt Inc., Dernbach, DE) essentially as described by Berne et al. and Hallett et al. [41, 42]. A dilution 1:10 of the original samples in water was placed in a quartz cuvette inside the apparatus to perform the light scattering measurement.

¹H High Resolution Magic Angle Spinning (HRMAS)

¹H HRMAS spectroscopy was performed using a Bruker Avance 11.7 T instrument equipped with a High Resolution Magic Angle Spinning (HRMAS) accessory, interfaced with a Linux driven Paravision IV console (Bruker BIOSPIN, Ettlingen, DE). Briefly, samples were dissolved in deuterated water (25 µL, 99.2% ²H, Apollo Scientific Limited, Stockport, UK) or deuterated chloroform (25 µL, 99.8% ²H, Scharlau, Barcelona, ES) containing 1 mM TMS (tetramethyl silane, Scharlau, Barcelona, ES) or 1 mM TSP (trimethyl silyl 2, 2', 3, 3' tetradeutero sodium propionate) as chemical shift references (0 ppm), respectively. Samples were placed in 50 µL zirconium rotors, inserted in the HRMAS probe and allowed 10 min for temperature equilibration. Water suppressed ¹H HRMAS spectra (4 °C, 4000 Hz) were acquired using the Carr-Purcell-Meiboom-Gil sequence with $\pi/2$ pulses, spectral width 10 kHz, acquisition time 0.41 sec, D1=1 sec, and 72 π pulses equally separated $\tau=1$ ms. Spectral processing used 1 Hz exponential line broadening function applied in the time domain data prior to Fourier Transformation [43].

2D COSY spectra were acquired using the sequence $\pi/2$ -TD- $\pi/2$ -acquire, with 2048 TD increments in the f_1 dimension and an acquisition time of 0,21s in the f_2 dimension. Cross-Peak correlations were analyzed in contour plots obtained after two dimensional Fourier transformations.

¹H NMR DOSY (Diffusion-Ordered NMR Spectroscopy) spectra of liposomal suspensions were acquired in a 400 MHz Bruker AVANCE III spectrometer (Bruker BIOSPIN, Ettlingen, DE) using a ¹H selective probe and 5 mm NMR tubes. The spin-echo

Stejskal-Tanner sequence, $\pi/2-\Delta-\pi-\Delta$ -acquire, was used with Δ values of 20, 50 and 100 ms and sixteen linear increments of the diffusion weighting gradient ranging from 2% to 95% of the maximal gradient strength. [43].

Water Relaxivity

We investigated the effect of magnetoliposomes on the T_1 and T_2 magnetic relaxation times of the water molecules of the suspension, to assess their potential usefulness as imaging agents for MRI detection. T_1 and T_2 relaxation times of magnetoliposomes were investigated in two different liposomal samples, containing or not the superparamagnetic particle Nanotex (0.5 mg Fe/mL). Dilutions of the original suspensions to 50% (v/v) and 25% (v/v) of the initial concentration were used to generate the relaxation vs. concentration profiles. $r_{1,2}$ relaxivity are the relaxation rates ($1/T_{1,2}$) of the water protons and can be calculated by linear regression fittings of the $r_{1,2}$ values to the Fe concentration using the expression

$$r_{1,2} = r_{0,2} + r_{1,2} [\text{Fe}]$$

where $r_{1,2}$ represent the relaxivity in r_1 or r_2 ($\text{s}^{-1} \text{mmol}^{-1}$); $r_{0,2}$, represents the relaxation rate of the water protons in the absence of magnetoliposomes, $r_{1,2}$ the relaxation rate of the water protons in the presence of different concentrations of magnetoliposomes, and $[\text{Fe}]$ the mM concentration of Fe in the magnetoliposomal suspension. Briefly, T_1 or T_2 values of all samples (37 °C) were measured using the inversion recovery sequence or Carr-Purcell-Meiboom-Gill (CPMG) sequences using a Bruker Minispec 1.5 Tesla time domain spectrometer (Bruker BIOSPIN, Ettlingen, DE) [44].

Fluorescence

We investigated the fluorescent properties of magnetoliposomes labeled with Rhodamine-100 chloride both *in vitro* and *in vivo* using an *in vivo* IVIS-Lumina system (Perkin Elmer, Waltham, Massachusetts, USA) [45]. *In vitro* and *in vivo* fluorescence images were acquired using a Green Fluorescent Protein filter (GFP, 445-490 nm excitations, 515-575 nm emission) during sixty seconds of exposure time. For the *in vitro* studies, three samples of liposomes containing or not the nanoparticle (25 mg Fe/mL) and the fluorescent dye (10 mg/mL), at different concentrations (18.75 mg Fe/mL, 12.5 mg Fe/mL, 6.25 mg Fe/mL for the nanoparticle and 7.5 mg/mL, 5 mg/mL, 2.5 mg/mL for Rhodamine-100) were placed in 96-well plate and scanned. For the *in vivo* studies, CD1 adult mice (30 g body weight) were anesthetized in a ventilated chamber with a mixture of oxygen and isoflurane (2%, Isoflo, Esteve, Barcelona, ES) and

maintained on it during the scanning period. Images were acquired as indicated above, five minutes before and three minutes after the i.p. injection (200 μL) of the liposomal preparations.

In vivo evaluation of anti-inflammatory activity

Animal Models of Inflammation and experimental design

All animal procedures were approved by the corresponding institutional ethical committee (INCSIC) and were performed in accordance with Spanish (law 32/2007) and European regulations (EU directive 86/609, EU decree 2001-486). Mice were housed in cages containing three or four animals per cage, under controlled temperature (23 °C) and humidity (47%) conditions and twelve hours light/dark cycles (8h, lights on).

A convenient model of colonic inflammation was induced in adult male C56BL6 mice (30 g body weight, Charles River, L'Arbresle, FR) through the administration of Dextran Sulfate sodium salt (DSS, Leti, Barcelona, ES) in the drinking water (3.5% w/v) during 5 days [46]. Briefly, two groups of mice received DSS treatment for five days and were injected in the tail vein (100 μL) with Phosphate Buffered Saline (n=6, Group 1), or Magnetoliposomes containing ω -3 PUFA-EE (n=6, Group 2) once during the first three days. The evolution of the body weight was followed daily in each mouse until the fifth day when the animals were investigated by MRI. For this purpose, mice were injected i.p. with 100 μL of Gd(III)DTPA (0.1 M) just before coronal T_{1w} images were acquired from the rectal zone of each mouse. Colonic inflammation was measured by the thickness of the rectal wall. After the MRI experiment, the administration of DSS was stopped and normal drinking water was administered to all mice, following their recovery in body weight until day 10th after DSS treatment initiation.

The model of oncologic inflammation was induced in CD1 mice (Charles River, L'Arbresle, FR) through the stereotaxic implantation of approximately 10^6 C6 glioma cells in the caudate nucleus of the mouse brain [47]. Fifteen days after the implantation, the tumor had proliferated reaching diameters in the range 5-15 mm. Five different treatments were applied intravenously on day 15th after implantation: Group 3 (n=4) received saline administrations only, Group 4 (n= 4) received a preparation of empty liposomes, Group 5, (n=4) received preparations of Magnetoliposomes without ω -3 PUFA-EE (100 μL) and Group 6 (n=4) preparations of Magnetoliposomes with PUFA-EE (100 μL), respectively. The growth of the glioblastoma after treatment was followed non-invasively in the same mouse on the day of

treatment initiation (Day 0) and three (Day 3) or six days (Day 6) after by T_{1w} (Gd(III) enhanced) and T_{2w} MRI.

We considered using administrations of free ω -3 PUFA-EE as controls for the liposomal administrations in both models. However, the need to formulate stable aqueous emulsions of ω -3 PUFA-EE micelles for intravenous administration, and the different physico-chemical and pharmacokinetic properties between micelles and liposomes limited the selection of free ω -3 PUFA-EE as control, favoring its liposomal formulation.

Magnetic Resonance Imaging

All MRI examinations were performed using a 7 Tesla horizontal magnet (16 cm bore) interfaced with a Bruker AVANCE III radiofrequency console operated through a Linux platform running Paravision V software (Bruker Biospin, Ettlingen, DE).

The colon inflammation model was explored with T_1 images using a Multi Slice Multi Echo (MSME) sequence, TE=10.643 ms, TR=521 ms, 3 averages, axial orientation, 22 slices, slice thickness 1.5 mm, interslice distance 1.5 mm, field of view 3.8 cm.

The glioma model was investigated with T_1 and T_2 weighted images. T_2 images were acquired using a Rapid Acquisition with Relaxation Enhancement (RARE) sequence, TE=14.77 ms, TR=2500 ms, 6 averages, axial direction, 14 slices, slice thickness 1 mm, interslice distance 1 mm, field of view 2.3 cm. T_1 images were acquired essentially using the similar conditions as for colonic inflammation with TR=350 ms, 14 slices, slice thickness 1 mm, interslice distance 1 mm, field of view 2.3 cm.

T_1 images were always obtained after the i.p. administration of 100 μ L of Gd(III)DTPA (0.1 M, Magnevist, Bayer Schering, Berlin, DE).

Statistical Analysis

Comparisons used the mean and standard deviation of all data from each group and the t-student test to assess significance ($p < 0.05$). Statistical analysis was done using SPSS software (IBM, New York, NY, US).

Results

Properties of the liposomal preparations.

Dynamic Light Scattering

The protocol for liposomal preparation originates a suspension of liposomes with homogenous size determined by the extrusion pore of the membrane. We determined experimentally the liposomal size by Dynamic Light Scattering (DLS). Figures 1C and 1D show representative results of size measurements by DLS in liposomal preparations without, or

with, ω -3 PUFA-EE, respectively. DLS analysis of liposomes without ω -3 PUFA-EE showed 200 nm diameter vesicles only, corresponding well with the 200 nm filter used in the extrusion process. The liposomal preparations containing ω -3 PUFA-EE showed, in addition to the expected 200 nm liposomal particles, larger particles of approximately 7000 nm. These microparticles accumulated with time at the top of the suspension as a lipid layer and could be easily removed from the preparation before further use. Smaller size vesicles of approximately 20-30 nm could also be detected by DLS.

Magnetic Resonance Spectroscopy

To elucidate the nature of the incorporation of ω -3 PUFA-EE into the liposomal suspensions we implemented a study using High Resolution Magic Angle Spinning 1 H Magnetic Resonance Spectroscopy (HRMAS).

Figure 2 shows representative 1 H HRMAS spectra from aqueous (Figure 2A, 2C) or chloroform (Figure 2B, 2D) suspensions of empty liposomes (left panels) and liposomes loaded with ω -3 PUFA-EE (right panels). The spectra of the chloroform suspensions show clearly resolved resonances from the magnetically different protons of L- α -phosphatidylcholine (PtdCho) and eicosapentaenoic acid (EPA, see Scheme 1 for the corresponding chemical structures). Complete assignments were achieved using literature values and confirmed experimentally by 2D COSY spectroscopy (Table 1) [48, 49]. The comparison of 1 H HRMAS spectra from aqueous suspensions of empty liposomes and liposomes containing ω -3 PUFA-EE demonstrates important differences. In particular, the 1 H HRMAS of empty liposome suspensions (Figure 2A) shows only small resonances from sufficiently mobile methyl (#1, Table 1) and methylene (#2, Table 1) protons of the sn_1 and sn_2 fatty acyl chains from L- α -phosphatidylcholine, most probably those located far away from the choline headgroup and closer to the center of the bilayer [50]. However, the motional restrictions of the bilayer arrangement impose the broadening and virtual disappearance of most phosphatidylcholine resonances, including particularly those of the choline headgroups (#6, Table 1) which are clearly observed in chloroform suspensions (Figure 2B, arrow) but not in aqueous suspension (Figure 2A, arrow). The insert in Figure 2A, illustrates the typical bilayer structure adopted by PtdCho molecules in liposomes with the choline headgroups oriented towards the external and internal aqueous interfaces. The insert in Figure 2B shows the PtdCho molecules in chloroform suspension adopting either the unimolecular or inverted micelle arrangements

with the sn_1 and sn_2 chains oriented towards the solvent.

The incorporation of ω -3 PUFA-EE (red molecules) into liposomes originates important spectral changes. Notably, most resonances of ω -3 PUFA-EE observed in chloroform (Figure 2D) become now observable in the aqueous suspension (Figure 2C). This means that the dynamics of ω -3 PUFA-EE are similar in aqueous and chloroform suspensions, indicating that ω -3 PUFA-EE may be present as stable nanogoticles in both cases. These findings were confirmed by the DLS measurements (Figure 1D) which revealed clearly the presence of sufficiently small, fast tumbling, PUFA-EE nanogoticles of approximately 30 nm diameter (see red nanogoticule in the Insert Figure 2C).

However, nanogoticule formation may not be the only form of ω -3 PUFA-EE integration in the lip-

osomes. Interestingly, note that resonance 20 in chloroform (Figure 2D), originated from the olefin protons (Table 1), is approximately three times higher than resonance 19 corresponding to the α -methylene protons of the ester group. Notably, the relative intensity of resonance 20 as compared to resonance 19, decreases drastically in the aqueous suspension (Figure 2C), suggesting a significant degree of immobilization of the olefinic protons from ω -3 PUFA-EE under these conditions. This finding is indeed compatible with a partial integration of the ω -3 PUFA-EE in the liposomal bilayer, a process involving the formation of an α -helical structure stabilizing the chain of conjugated double bonds within the membrane, resulting in partial immobilization and 1H NMR invisibility [51, 52]. This is illustrated in the insert of Figure 2C by the red molecules of ω -3 PUFA-EE inserted in the bilayer membrane.

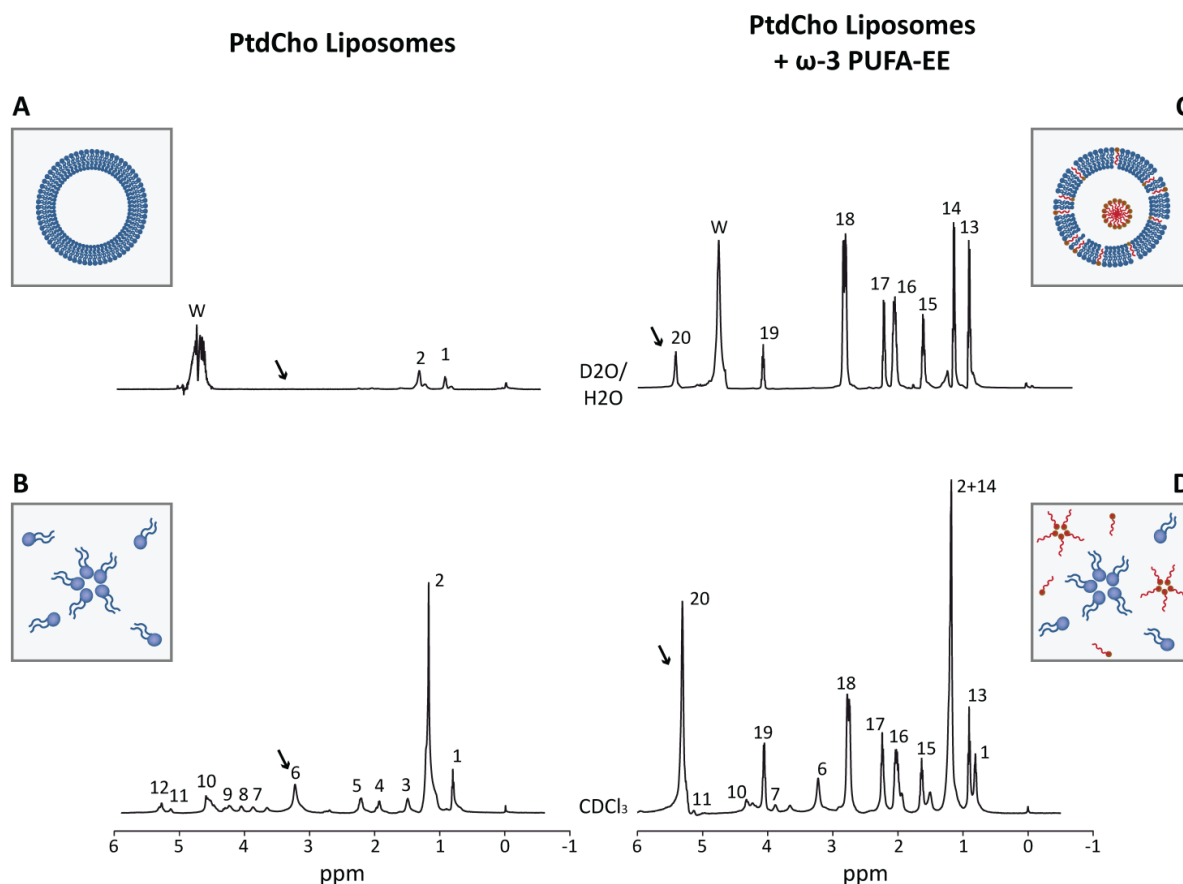
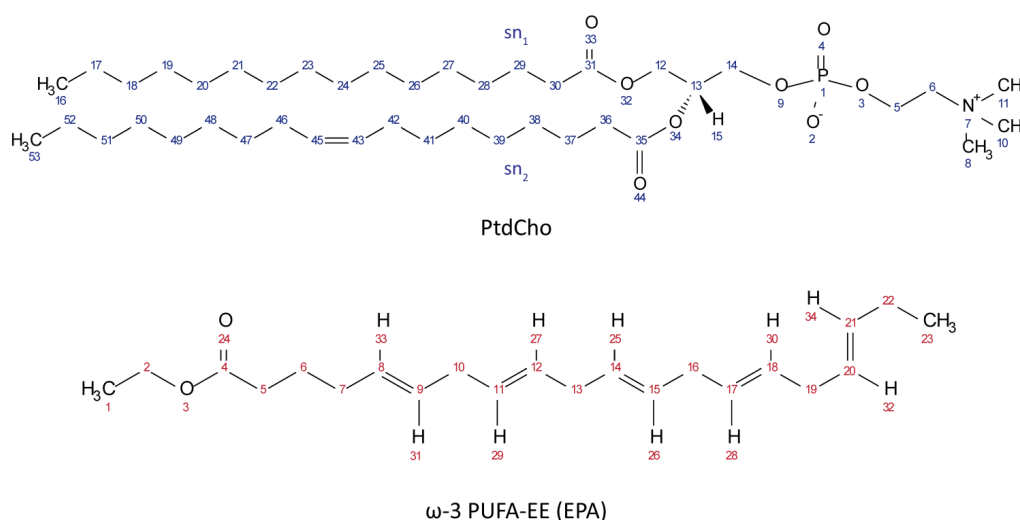


Figure 2. Characterization of liposomes loaded with ω -3 PUFA-EE by Magnetic Resonance Spectroscopy. Representative HRMAS spectra (500.13 MHz, 4 °C, 4000 Hz rotation) of aqueous (A, C) and chloroform (B, D) suspensions from empty liposomes (A, B) and from liposomes loaded with ω -3 PUFA-EE (C, D). Resonance numbers refer to the assignments indicated in Table 1 and the structures depicted in Scheme 1. Inserts A and B depicts schematically the organization of PtdCho molecules (blue) in the bilayer structure of aqueous liposomal suspensions or in the chloroform suspension as individual PtdCho molecules or inverted micelles with the choline headgroups oriented inwards. Inserts C or D illustrate the localization of ω -3 PUFA-EE inserted in the membrane or nanogoticles in the lumen of aqueous liposomal suspensions, or the inverted micelles and free molecules of PtdCho and ω -3 PUFA-EE in chloroform suspensions, respectively.



Scheme 1. Chemical Structures of PtdCho (top, blue protons) and ω -3 PUFA-EE (bottom, red protons).

Table 1. Assignments of phospholipid and ω -3 PUFA-EE ^1H NMR resonances in water and chloroform suspensions.

	Resonance number	Assignment ^{a)}	$\delta_{\text{H}_2\text{O}}^{\text{b)}$	$\delta_{\text{CDCl}_3}^{\text{c)}$
Liposomes	1	H ₁₆ , H ₅₃	0.9	0.89-0.86 (m)
	2	H ₁₇₋₂₈ , H ₃₈₋₄₁ , H ₄₇₋₅₂	1.32	1.25 (m)
	3	H ₂₉ , H ₃₇	n.o. ^{d)}	1.57 (m)
	4	H ₄₂₋₄₆	n.o. ^{d)}	2.02 (m)
	5	H ₃₀ , H ₃₆	n.o. ^{d)}	2.34-2.26 (dt)
	6	H ₈ , H ₁₀ , H ₁₁	n.o. ^{d)}	3.28 (t)
	7	H ₆	n.o. ^{d)}	3.77 (t)
	W	Water	4.79	-
	8	H ₁₂	n.o. ^{d)}	4.05 (m)
	9	H ₁₄	n.o. ^{d)}	4.13 (m)
ω -3 PUFA-EE	10	H ₅	n.o. ^{d)}	4.37 (m)
	11	H ₁₅	n.o. ^{d)}	5.23 (m)
	12	H ₄₃ , H ₄₅	n.o. ^{d)}	5.33 (m)
	13	H ₂₃	1.03	0.97 (t)
	14	H ₁	1.27	1.25 (t)
	15	H ₆	1.73	1.7 (q)
	16	H ₇ , H ₂₂	2.19-2.14	2.32-2.07 (m)
	17	H ₅	2.32	2.3 (t)
	18	H ₁₀ , H ₁₃ , H ₁₆ , H ₁₉	2.9-2.87	2.85-2.8 (m)
	19	H ₂	4.12	4.12 (t)
W	Water	4.79	-	
20	H ₂₅₋₃₄	5.46-5.40	5.38-5.30 (m)	

^{a)} Resonances 1-20 in Figure 2 are assigned to specific protons of the corresponding PtdCho and ω -3 PUFA-EE molecules (see Scheme 1 for proton numbering).

^{b)} Chemical shifts are measured in ppm and referenced to TSP at 0 ppm.

^{c)} Chemical shifts are measured in ppm and referenced to TMS at 0 ppm.

^{d)} The resonances marked with "n.o." are not observable by high resolution ^1H HRMAS because of dynamical restrictions in the bilayer.

The above mentioned experiments do not clarify the intraluminal or extraliposomal localization of the nanogoticules. To investigate this aspect we performed Diffusion Weighted Spectroscopy experiments (DOSY, Figure 3) [53]. This approach measures the Apparent Diffusion Coefficient of water (ADC) in the liposomal preparation. According to the Einstein's principle the ADC is inversely proportional to the number of molecular obstructions that the water molecule would find along its random mean diffusional path [54]. ADC measurements under these

conditions are known to be dominated by the contribution of the extraliposomal volume and if goticules would be present there at a significant proportion, one would expect a decrease in the observed ADC. In contrast, if goticules would be located inside the liposomes, no additional obstructions would be found, because of the small contribution of the lumen space to total volume of the suspension, and consequently, very similar ADC's would be measured in the presence and absence of ω -3 PUFA-EE. We found no significant differences in the water ADCs values between both preparations at the three diffusion times investigated, suggesting that the fatty acids ester nanodroplets do not increase significantly the molecular obstructions to water movements. Since the ADCs are primarily dominated by those of the extraliposomal volume, our results suggest that most PUFA-EE goticules are localized in the intraluminal space.

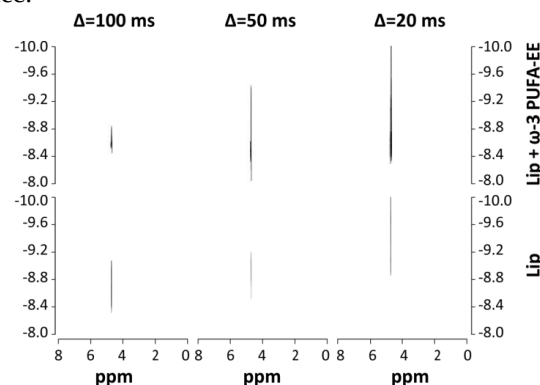


Figure 3. Characterization of PUFA-EE nanogoticule localization. ^1H NMR DOSY (400,7 MHz, 22 °C) spectra of translational water diffusion in liposomal suspensions at different diffusion times Δ . Spectra were obtained from liposomal suspensions loaded (top panels) or not (bottom panels) with ω -3 PUFA-EE, with Δ of 100 ms (left), 50 ms (center) and 20 ms (right). Note that the presence of ω -3 PUFA-EE does not decrease significantly the water ADC at any of the diffusion times investigated, suggesting primarily an intraluminal location of the goticules.

This could be directly demonstrated by the ultrafiltration experiments in which the goticules of ω -3 PUFA-EE model suspensions passed easily and quite completely the 300 kD filters, while the suspensions of liposomes containing ω -3 PUFA-EE did not pass through filters of identical dimensions, retaining most of the PUFA-EE goticules. This confirmed that ω -3 PUFA-EE goticules are predominantly intraluminal as indicated by the water ADC measurements.

Taking together these evidences allow for the conclusion that liposomal loading with ω -3 PUFA-EE, involves both, the formation of nanogoticules located in the liposomal lumen as well as the integration of ω -3 PUFA-EE within the liposomal bilayer.

Magnetic relaxation properties

We investigated the T_1 and T_2 magnetic relaxation properties of water molecules in suspensions of liposomes, containing or not Nanotex. Tables 2 and 3 summarize these results.

Table 2 shows the values of the T_1 water relaxation time in liposome suspensions containing or not Nanotex in three successive dilutions of the initial concentration. The T_1 relaxation value is shortest for the highest Nanotex concentration, increasing approximately linearly when suspensions are further diluted, giving a relaxivity value r_1 of 6.26 $\text{mM}^{-1}\text{s}^{-1}$. The same situation is observed with empty liposomes, albeit with a much smaller slope for the increase in T_1 relaxation time due to the absence of the superparamagnetic nanoparticle.

Table 3 shows the results of T_2 water relaxation measurements in the different samples. T_2 values for the original sample with Nanotex depicted approximately one thousand times faster relaxation than the empty liposomes (Table 3). The T_2 relaxation value is shortest for the highest Nanotex concentration and increases approximately linearly when the liposomal suspensions are diluted, giving a relaxivity value r_2 of

64.6 $\text{mM}^{-1}\text{s}^{-1}$. The same situation is observed with empty liposomes, albeit with a much lower increase of T_2 relaxation upon dilution and significantly smaller relaxivity. In summary, the relaxivity value r_1 increases from 0.55 $\text{mM}^{-1}\text{s}^{-1}$ for free Nanotex [38] in suspension to 6.26 $\text{mM}^{-1}\text{s}^{-1}$ for Nanotex encapsulated in liposomes. In the case of r_2 , the value of 88.97 $\text{mM}^{-1}\text{s}^{-1}$ for free Nanotex [38] in solution decreases to 64.61 $\text{mM}^{-1}\text{s}^{-1}$ for encapsulated Nanotex.

Fluorescence *in vitro* and *in vivo*

The capacity of liposomes as optical biomarkers was tested using *in vitro* and *in vivo* fluorescence. Figure 4 summarizes the results obtained *in vitro* and *in vivo* with liposomes containing or not Nanotex, and labeled fluorescently with Rhodamine-100.

Table 2. T_1 values of aqueous liposomal suspensions containing or not Nanotex in decreasing concentrations.

Suspension type / dilution ^{a)}	T_1 (ms) ^{b)}		
	x1	x1/2	x1/4
Liposomes w/ nanoparticles	17.3 ± 0.0	34.2 ± 0.1	64.1 ± 0.1
Liposomes w/o nanoparticles	2161.7 ± 154.6	2207.3 ± 107.9	2955.0 ± 7.1

^{a)} The dilutions (v/v) of the liposomal preparations correspond to the original liposomal suspension (5.26 mM PtdCho, x1), 50% (x1/2) or 25% (x1/4). In the liposomal preparations containing Nanotex these dilutions correspond to iron concentrations of 0.5 mg Fe/mL, 0.25 mg Fe/mL and 0.125 mg Fe/mL.

^{b)} T_1 values were determined at 1.5 Tesla (22 °C, Bruker Minispec, Rheinstetten, DE) using the inversion recovery sequence.

Table 3. T_2 values of aqueous liposomal suspensions containing or not Nanotex in decreasing concentrations.

Suspension type / dilution ^{a)}	T_2 (ms) ^{b)}		
	x1	x1/2	x1/4
Liposomes w/ nanoparticles	1.7 ± 0.0	3.5 ± 0.0	6.6 ± 0.0
Liposomes w/o nanoparticles	1138.3 ± 34.6	1034.3 ± 6.1	2228.2 ± 0.1

^{a)} The dilutions (v/v) of the liposomal preparations correspond to the original liposomal suspension (5.26 mM PtdCho, x1), 50% (x1/2) or 25% (x1/4). In the liposomal preparations containing Nanotex these dilutions correspond to iron concentrations of 0.5 mg Fe/mL, 0.25 mg Fe/mL and 0.125 mg Fe/mL.

^{b)} T_2 values were determined at 1.5 Tesla (22 °C, Bruker Minispec, Rheinstetten, DE) using the inversion recovery sequence.

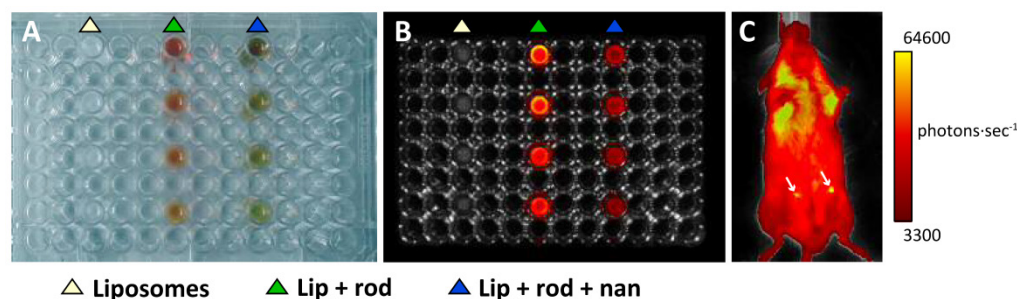


Figure 4. Fluorescence imaging of liposomes. *In vitro* (A, B) and *in vivo* (C) fluorescence images of liposomes loaded with nanoparticles and Rhodamine-100 as acquired with an IVIS-Lumina camera. A: Visible picture of the 96 well plate used as phantom, showing the columns of wells loaded with decreasing concentrations (top to bottom) of empty liposomes (white triangle), liposomes loaded with Rhodamine-100 (green triangle) and liposomes loaded with Rhodamine-100 and Nanotex (blue triangle). B: Fluorescence image of the same phantom using the Green Fluorescent Protein (GFP) filter. Note the increased fluorescence of the liposomes containing Rhodamine-100 only as compared to those containing Rhodamine-100 and Nanotex. C: *In vivo* images of a mouse injected with liposomes containing Rhodamine-100 and Nanotex (left side arrow), or liposomes containing Rhodamine-100 only (right side arrow).

Figures 4A-B show results obtained in an *in vitro* fluorescence experiment, comparing in a multiwell plate, the fluorescence of empty liposomes (left track, white triangle), liposomes containing Rhodamine-100 (central track, green triangle) and liposome containing Rhodamine-100 and Nanotex (right track, blue triangle). Liposomes containing only Rhodamine-100 present more intense fluorescence than liposomes containing both Rhodamine-100 and Nanotex. This may be due to either or both of two circumstances. First, liposomes with Nanotex have to share their lumen space with Rhodamine-100 and one or more nanoparticles, resulting in a smaller intraluminal volume available for Rhodamine-100 accumulation and thus decreased intraluminal Rhodamine-100 concentration. Second, the Nanotex acrylic acid coating or its magnetite core could partially quench the fluorescence of Rhodamine-100.

Figure 4C shows the results of a representative *in vivo* experiment in a mouse receiving an i.p. injection of liposomes labeled with Rhodamine-100 containing (left) or not (right) Nanotex. As in the *in vitro* experiments, liposomes with Nanotex and Rhodamine-100 (left) depict less quantum efficiency than liposomes with only Rhodamine-100, however, they still become observable by *in vivo* fluorescence (Figure 4C).

Anti-inflammatory effects in vivo

Mouse model of colonic inflammation

We investigated the anti-inflammatory effects of liposomal preparations containing or not ω -3 PUFA-EE using a well-established model of colonic inflammation induced by dextran sulfate (sodium salt, DSS) administration [46, 55]. Untreated mice showed significant decreases in body weight, while mice treated with magnetoliposomes containing ω -3 PUFA-EE reduced appreciably the loss of body weight along the treatment period (not shown), revealing a potent anti-inflammatory effect of the formulation.

Figure 5 shows representative results of the administration of saline (Figure 5A) or magnetoliposomes containing ω -3 PUFA-EE (Figure 5B) to mice with rectal inflammation induced by DSS. Saline treated mice showed, as expected, clearly increased colonic wall thickness, easily observable in T_{1w} images after Gd(III)DTPA enhancement. However, mice treated with magnetoliposomes containing ω -3 PUFA-EE (Figure 5B) depicted a significant reduction in colonic wall thickness, revealing a prominent anti-inflammatory effect of the theranostic formulation (Figure 5C-D). Notably, treatment with magnetolip-

osomes resulted, not only in a reduction of the rectal wall thickness, but in a significant darkening of this structure, a clear indication of the presence of magnetoliposomes in the inflamed region.

C6 glioma mouse model

We then examined the effects of magnetoliposomes containing or not ω -3 PUFA-EE in the inflammation associated to glioma growth [8], using the C6 glioma models.

Figure 6 shows representative MRI T_{1w} images of glioma evolution in a mouse treated with magnetoliposomes containing (bottom panels) or not (upper panels) ω -3 PUFA-EE. Mice receiving magnetoliposomes without ω -3 PUFA-EE developed tumors to the same extent than controls receiving saline (not shown). However, mice receiving magnetoliposomes containing ω -3 PUFA-EE decreased notably the rate of glioma growth, and even increased the regression rate of the implanted gliomas. Table 4 compares the effects of administering magnetoliposomes containing ω -3 PUFA-EE with control administrations of saline, empty liposomes or liposomes containing Nanotex only. The data show that the administration of magnetoliposomes containing ω -3 PUFA EE to mice bearing C6 tumors preserved the life of mice and induced a decrease in tumor size, while the administration of saline, empty liposomes or magnetoliposomes containing only Nanotex did not preclude death of the animals nor reduced tumor growth.

Table 4. Assessment of C6 tumor growth in mice receiving magnetoliposomes containing or not ω -3 PUFA-EE.

Type of liposomal preparation injected ^{a)}	Mouse ^{b)}	Initial size (mm ²) ^{c)}	Final size (mm ²) ^{d)}	% increase or decrease tumor size after treatment
None, saline	Mouse 1	12.72	18.87	+48.35%
	Mouse 2	38.89	131.82	+238.96%
Empty Liposomes	Mouse 5	13.46	26.92	+200,00%
	Mouse 6	18.37	76.23	+414,90%
Nanotex Liposomes	Mouse 9	15.756	27.5	+74.54%
	Mouse 10	14.473	20.212	+39.65%
	Mouse 11	8.298	13.787	+66.15%
Nanotex + ω -3 PUFA-EE Liposomes	Mouse 13	12.624	2.825	-77.62%
	Mouse 14	6.07	0.396	-93.48%
	Mouse 15	8.952	0.347	-96.12%
	Mouse 16	24.377	10.179	-58.24%

^{a)} Liposomal preparations were administered i.v. through the tail vein fifteen days after C6 cell implantation.

^{b)} Groups containing four mice at the time of treatment initiation were used in all conditions. Only the mice surviving six days after treatment initiation are shown.

^{c)} Tumor size before treatment initiation.

^{d)} Tumor size after six days of treatment.

^{e-d)} Tumor area (mm²) reflects the area including the tumor and peripheral inflammation as detected in coronal cross sections of T_{2w} images obtained before (initial) or six days after (final) treatment.

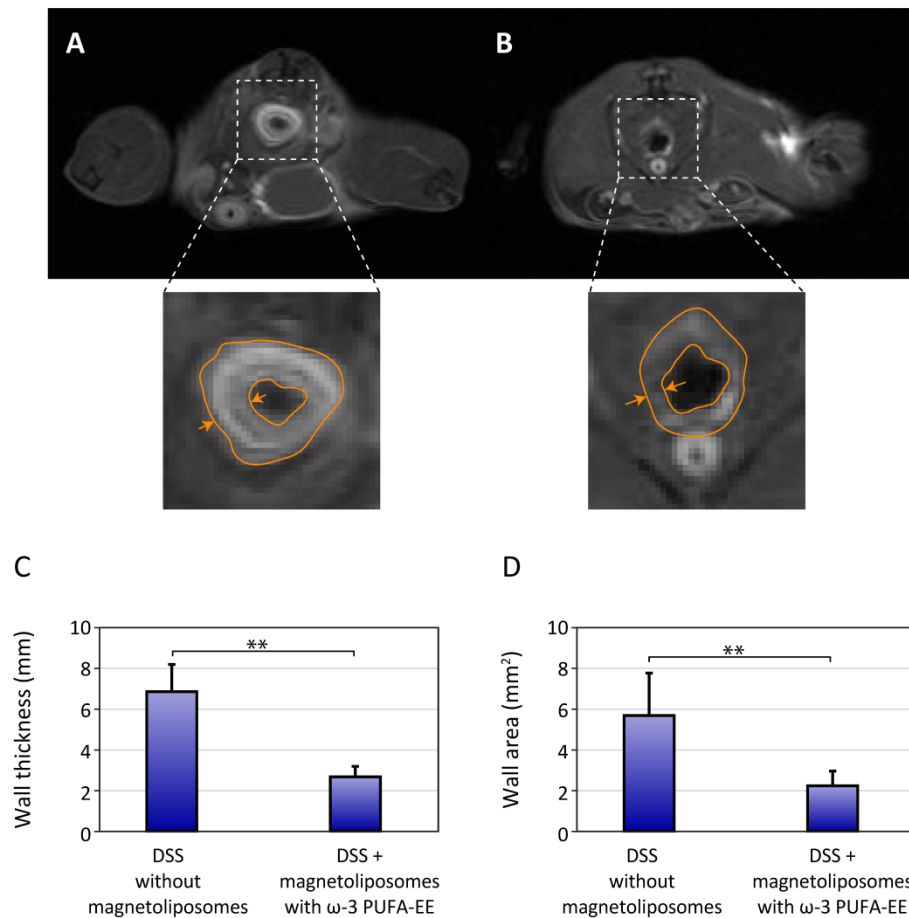


Figure 5. Theranostic effects on colonic inflammation. T_{1w} MRI of colonic inflammation in the rectal region of mice subjected to oral DSS administration for five days. A: untreated, B: treated with liposomes loaded with Nanotex and ω -3 PUFA-EE. Note the darker appearance of the rectum (arrows) from the mouse receiving magnetoliposomes loaded with Nanotex, revealing the presence of the nanoparticle. Wall thickness is illustrated by the orange line. Mean and standard deviation from measurements of rectal wall thickness (C) and wall area (D) are shown under the different conditions.

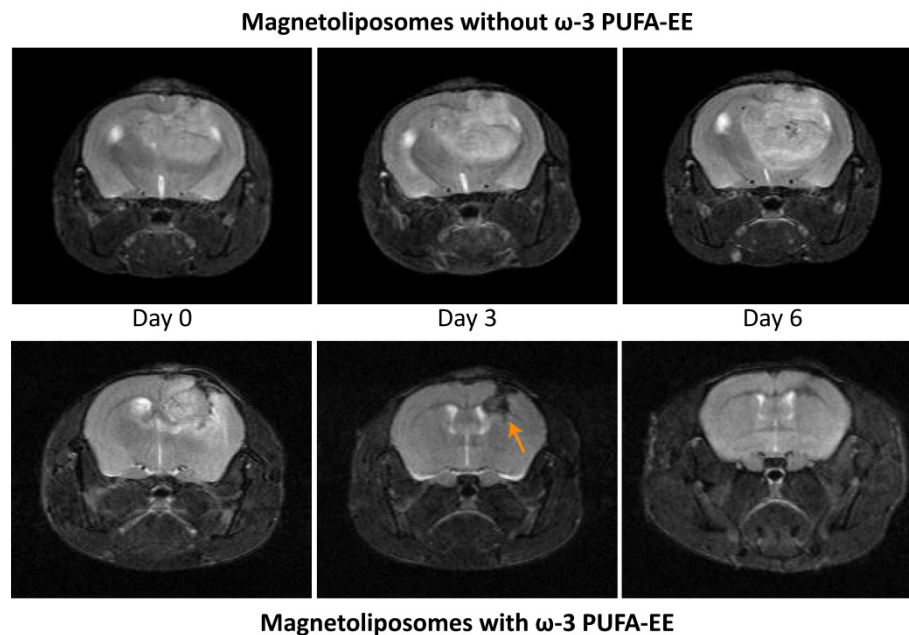


Figure 6. Theranostic effects on tumoral inflammation and growth. Effect of magnetoliposomal preparations containing (bottom) or not (top) ω -3 PUFA-EE on the time course of glioma development after implantation of C6 cells in the caudate nucleus of the mouse brain. T_{2w} images were acquired as indicated in methods. Left panels: (day 0), central panels (day 3), right panels (day 6). Note the accumulation of magnetoliposomes loaded with PUFA-EE revealed by the darkening of the tumoral lesion (arrow) and the eventual disappearance of the tumor six days after treatment. Table 4 summarizes the results obtained with animals surviving day 6.

In addition to the MRI results, it becomes important to comment the external aspect and behavior of the mice. Mice with no treatment depicted bristly hair, decrease in motor activity and eventually hemiplegia and hemiparesis. Mice treated with liposomes with PUFA-EE did not present such symptoms, revealing significantly better physiopathological state and sometimes regression of the tumor.

Discussion

We have presented a novel liposomal formulation combining the therapeutic properties of ω -3 PUFA-EE with the non-invasive multimodal imaging capabilities of Nanotex and Rhodamine-100, or the combination of both.

Interestingly, the encapsulation of a superparamagnetic nanoparticle in a liposome results in different relaxivity properties as compared to those of the free nanoparticle in suspension. These changes reflect necessarily modifications in the dynamics of the nanoparticle-water interaction induced by the encapsulation process. Indeed it would be expected that the encapsulation would decrease the interaction of the nanoparticle with the surrounding solvent water, because of the water impermeable liposomal membrane. These reduction effects are expected to occur mainly in the "outer sphere" relaxivity component, representing approximately 50% of the total relaxivity [56, 57]. The approximately 30% decrease observed in r_2 follows closely enough this interpretation. However, a similar decrease would also be expected to occur in r_1 . This is not observed, indicating that the "outer sphere" effect is not the only determinant of the changes in relaxivity occurring after liposomal encapsulation. The r_1 value shows, in contrast, an important increase, larger than an order of magnitude. The most probable cause of this increase is the restriction in the rotational movement of the nanoparticle when present in the encapsulated lumen environment. This may be imposed by, either an association to the liposomal membrane, an increase in intraluminal microviscosity, or binding or interaction with neighboring nanoparticles, resulting in a slower tumbling time (τ_r in [57]). Indeed r_1 and r_2 have different determinants and behavior, as explained from their different Solomon-Bloembergen-Morgan equations [57-60], and it is not surprising that they respond differently to encapsulation. Moreover, r_1 and r_2 reflect the different time scales of T_1 (s) and T_2 (ms), making easier to understand that the events occurring in the ms range of T_2 , may be too fast to be detected in the second range time-scale of T_1 . In summary, the encapsulation of Nanotex in liposomes appears to decrease the "outer sphere" contribution, reflecting water diffusional limitations imposed by the liposo-

mal membrane, and a decrease in the tumbling time of the nanoparticle, revealing associations to the liposomal membrane or to other nanoparticles in the lumen. In this respect, our results are similar to those previously described in literature [61-63].

Present results on the encapsulation of ω -3 PUFA-EE in liposomes complement and extend previous studies [64-66]. Our results show that it is possible to encapsulate significant amounts of lipid soluble ω -3 PUFA-EE goticules in the liposomal lumen. This can be observed by the prominent ^1H HRMAS resonances of liposomal suspensions containing the encapsulated fatty acids. The fact that these resonances are observed reveals that the ω -3 PUFA-EE are mainly present as small, fast tumbling nanogoticules in the liposomal lumen. This is because ω -3 PUFA-EE nanogoticules pass easily through 300 kD filters, while the encapsulated ω -3 PUFA-EE goticules, are retained by the same filters together with the liposomes. This finding is further confirmed by the fact that liposomal preparations containing encapsulated ω -3 PUFA-EE show the same ADC as the empty liposomal preparations, revealing that the obstructions caused by the presence of ω -3 PUFA-EE goticules do not contribute appreciably to the average ADC of the suspension, dominated by the extraliposomal compartment.

Our results provide also evidence that a significant portion of the encapsulated ω -3 PUFA-EE is inserted within the liposomal bilayer. This is because the ω -3 PUFA-EE molecules inserted in the membrane adopt an α -helical structure around the olefinic protons [51], becoming rotationally immobilized and ^1H HRMAS undetectable [52]. This circumstance is easily observed in resonance 20 (Figure 2C-2D), which shows full intensity in chloroform and roughly 30% intensity in water. This suggests that approximately 70% of encapsulated ω -3 PUFA-EE becomes inserted in the membrane and ^1H HRMAS invisible, while 30% forms ^1H HRMAS observable nanogoticules in the liposomal lumen.

The fluorescence study shows (Figure 4C) that the in vivo fluorescence signal from Rhodamine-100 contained in magnetoliposomes is weak, superimposes on significant endogenous fluorescence and fades away progressively when the liposomes distribute later over a larger volume, as in colonic inflammation models. Moreover, the presence of Nanotex quenches considerably the fluorescence of Rhodamine-100 (Figure 4B), making in vivo fluorescence detection not advisable for this agent under the present conditions. Furthermore, in vivo fluorescence applications to the brain are largely limited by the presence of the skull, an opaque bone structure hampering severely fluorescence detection. Taken togeth-

er, the reduced fluorescence of our nanoparticles and the presence of the skull, dissuaded further fluorescence applications to the brain.

We show here also that the magnetoliposomal preparations containing Nanotex and ω -3 PUFA-EE present prominent anti-inflammatory activities against colonic inflammation and important anti-tumoral effects against glioma while becoming simultaneously observable in vivo by MRI.

Colonic inflammation is a disease associated to ulcerative colitis and Chron's disease, two incurable pathologies at present. These are treated currently with conventional anti-inflammatory therapies, mainly free steroidal or immunosuppressant drugs, and eventually colonic resection by surgery [67]. The formulation proposed here has been shown to become therapeutically useful in animal models of DSS intoxication, adding a new, non-toxic formulation to the arsenal of therapeutic methods against these two morbid and prevalent diseases.

Finally, our liposomal formulation encapsulating ω -3 PUFA-EE and Nanotex has demonstrated valuable effects against glioma C6, slowing down proliferation and even inducing remission. These effects are due to the combination of Nanotex and the ω -3 PUFA-EE since they are not induced by empty liposomes or liposomes containing ω -3 PUFA-EE only. The precise mechanism of this unexpected cooperative effect remains to be elucidated, but could probably involve a significant decrease in the pro-inflammatory component required for glioma proliferation or invasion and iron modulation of reactive oxygen species [8, 9, 68].

In summary, present results illustrate the properties and use of a new nanotechnological formulation including one or more imaging agents and a therapeutic ω -3 PUFA-EE, useful in the treatment of the inflammatory component of colonic inflammation or glioma in animal models. A patent has been filed protecting the preparation, properties and use of this formulation [69].

Abbreviations

ADC: apparent diffusion coefficient; COSY: correlation spectroscopy; CPMG: Carr-Purcell-Meiboom-Gill; DLS: dynamic light scattering; DOSY: diffusion ordered NMR spectroscopy; DTPA: diethylenediamine pentaacetic acid; EPR: enhanced permeability retention; GFP: green fluorescent protein; HRMAS: high resolution magic angle spinning; i.p.: intraperitoneal; i.v.: intravenously; MRI: magnetic resonance imaging; MSME: multi slice multi echo; NMR: nuclear magnetic resonance; PAA: poly(acrylic acid); PtdCho: L- α -phosphatidylcholine; PUFA-EE: polyunsaturated fatty acid ethyl ester; RARE: rapid acquisition with

relaxation enhancement; T_1 : longitudinal relaxation time; T_2 : transversal relaxation time; T_{1w} : image weighted in longitudinal relaxation time; T_{2w} : image weighted in transversal relaxation time; TMS: tetramethyl silane; TSP: trimethyl silyl-2, 2', 3, 3'tetra-deutero- sodium propionate.

Acknowledgements

Authors wish to express their gratitude to Drs. Gerard Bannenberg and Fernando Moreno and Mrs. Iratxe Cano from SOLUTEX SL, for useful discussions and advise during the progression of the work. We are also indebted to Mr. Javier Pérez CSIC for professional drafting of the illustrations, and to Mrs. Patricia Sánchez CSIC, for expert and dedicated technical assistance.

In memory of Prof. Manuel Rico.

Funding

This work was supported in part by grants from SOLUTEX SL to SC, grants from the Spanish Ministry of Economy and Competitiveness SAF2011-23622, IPT-2012-1331-006000 to SC, grant CTQ2013-47669-R to PB, and grant S2010/BMD-2349 from the Community of Madrid to S.C. and P.B. D.C. and V.N. held predoctoral contracts from Agencia Estatal Consejo Superior de Investigaciones Científicas (CSIC).

Competing Interests

The authors have declared that no competing interest exists.

References

- Libby P, Ridker PM, Maseri A. Inflammation and atherosclerosis. *Circulation*. 2002; 105: 1135-43.
- Libby P, Lichtman AH, Hansson GK. Immune effector mechanisms implicated in atherosclerosis: from mice to humans. *Immunity*. 2013; 38: 1092-104.
- McGeer PL, McGeer EG. The inflammatory response system of brain: implications for therapy of Alzheimer and other neurodegenerative diseases. *Brain Res Rev*. 1995; 21: 195-218.
- McGeer PL, McGeer EG. The amyloid cascade-inflammatory hypothesis of Alzheimer disease: implications for therapy. *Acta Neuropathol*. 2013; 126: 479-97.
- Wellen KE, Hotamisligil GS. Inflammation, stress, and diabetes. *J Clin Invest*. 2005; 115: 1111-9.
- Donath MY, Dalmas E, Sauter NS, Boni-Schnetzler M. Inflammation in obesity and diabetes: islet dysfunction and therapeutic opportunity. *Cell Metab*. 2013; 17: 860-72.
- Williams CS, Mann M, DuBois RN. The role of cyclooxygenases in inflammation, cancer, and development. *Oncogene*. 1999; 18: 7908-16.
- Coussens LM, Werb Z. Inflammation and cancer. *Nature*. 2002; 420: 860-7.
- Coussens LM, Zitvogel L, Palucka AK. Neutralizing tumor-promoting chronic inflammation: a magic bullet? *Science*. 2013; 339: 286-91.
- Meade EA, Smith WL, DeWitt DL. Differential inhibition of prostaglandin endoperoxide synthase (cyclooxygenase) isozymes by aspirin and other non-steroidal anti-inflammatory drugs. *J Biol Chem*. 1993; 268: 6610-4.
- Lands LC, Stanojevic S. Oral non-steroidal anti-inflammatory drug therapy for lung disease in cystic fibrosis. *Cochrane Database Syst Rev*. 2013; 6: CD001505.
- Lee CL, Hwang TL, He WJ, Tsai YH, Yen CT, Yen HF, et al. Anti-neutrophilic inflammatory steroidal glycosides from *Solanum torvum*. *Phytochemistry*. 2013; 95: 315-21.
- Henry D, Lim LL, Garcia Rodriguez LA, Perez Gutthann S, Carson JL, Griffin M, et al. Variability in risk of gastrointestinal complications with individual non-steroidal anti-inflammatory drugs: results of a collaborative meta-analysis. *BMJ*. 1996; 312: 1563-6.
- McGettigan P, Henry D. Use of non-steroidal anti-inflammatory drugs that elevate cardiovascular risk: an examination of sales and essential medicines

- lists in low-, middle-, and high-income countries. *PLoS Med.* 2013; 10: e1001388.
15. Lian T, Ho RJ. Trends and developments in liposome drug delivery systems. *J Pharm Sci.* 2001; 90: 667-80.
 16. Torchilin VP. Recent advances with liposomes as pharmaceutical carriers. *Nature Reviews Drug Discovery.* 2005; 4: 145-60.
 17. Kluzka E, Yeo SY, Schmid S, van der Schaft DW, Boekhoven RW, Schiffelers RM, et al. Anti-tumor activity of liposomal glucocorticoids: The relevance of liposome-mediated drug delivery, intratumoral localization and systemic activity. *J Control Release.* 2011; 151: 10-7.
 18. Hilgenbrink AR, Low PS. Folate receptor-mediated drug targeting: from therapeutics to diagnostics. *J Pharm Sci.* 2005; 94: 2135-46.
 19. Danhier F, Feron O, Preat V. To exploit the tumor microenvironment: Passive and active tumor targeting of nanocarriers for anti-cancer drug delivery. *J Control Release.* 2010; 148: 135-46.
 20. Pan J, Wan D, Gong J. PEGylated liposome coated QDs/mesoporous silica core-shell nanoparticles for molecular imaging. *Chem Commun (Camb).* 2011; 47: 3442-4.
 21. Petersen AL, Hansen AE, Gabizon A, Andresen TL. Liposome imaging agents in personalized medicine. *Adv Drug Deliv Rev.* 2012; 64: 1417-35.
 22. Liu G, Moake M, Har-el Y-e, Long CM, Chan KW, Cardona A, et al. In vivo multicolor molecular MR imaging using diamagnetic chemical exchange saturation transfer liposomes. *Magn Reson Med.* 2012; 67: 1106-13.
 23. Soenen SJ, Hødenius M, De Cuyper M. Magnetoliposomes: versatile innovative nanocolloids for use in biotechnology and biomedicine. *Nanomedicine (Lond).* 2009; 4: 177-91.
 24. Garg T, K Goyal A. Liposomes: Targeted and Controlled Delivery System. *Drug Delivery Letters.* 2014; 4: 62-71.
 25. Lammers T, Kiessling F, Hennink WE, Storm G. Nanotheranostics and image-guided drug delivery: current concepts and future directions. *Mol Pharm.* 2010; 7: 1899-912.
 26. Al-Jamal WT, Kostarelos K. Liposomes: from a clinically established drug delivery system to a nanoparticle platform for theranostic nanomedicine. *Acc Chem Res.* 2011; 44: 1094-104.
 27. Lammers T, Aime S, Hennink WE, Storm G, Kiessling F. Theranostic nanomedicine. *Acc Chem Res.* 2011; 44: 1029-38.
 28. Langereis S, Geelen T, Grull H, Strijkers GJ, Nicolay K. Paramagnetic liposomes for molecular MRI and MRI-guided drug delivery. *NMR Biomed.* 2013; 26: 728-44.
 29. Simopoulos AP. Omega-3 fatty acids in health and disease and in growth and development. *Am J Clin Nutr.* 1991; 54: 438-63.
 30. Simopoulos AP. Omega-3 fatty acids in inflammation and autoimmune diseases. *J Am Coll Nutr.* 2002; 21: 495-505.
 31. Mori TA, Beilin LJ. Omega-3 fatty acids and inflammation. *Curr Atheroscler Rep.* 2004; 6: 461-7.
 32. Calder PC. n-3 polyunsaturated fatty acids, inflammation, and inflammatory diseases. *Am J Clin Nutr.* 2006; 83: 1505S-19S.
 33. Wall R, Ross RP, Fitzgerald GF, Stanton C. Fatty acids from fish: the anti-inflammatory potential of long-chain omega-3 fatty acids. *Nutr Rev.* 2010; 68: 280-9.
 34. Zhang W, Hu X, Yang W, Gao Y, Chen J. Omega-3 polyunsaturated fatty acid supplementation confers long-term neuroprotection against neonatal hypoxic-ischemic brain injury through anti-inflammatory actions. *Stroke.* 2010; 41: 2341-7.
 35. Calder PC. Fatty acids and inflammation: the cutting edge between food and pharma. *Eur J Pharmacol.* 2011; 668 Suppl 1: S50-8.
 36. Langman MJ, Weil J, Wainwright P, Lawson DH, Rawlins MD, Logan RF, et al. Risks of bleeding peptic ulcer associated with individual non-steroidal anti-inflammatory drugs. *Lancet.* 1994; 343: 1075-8.
 37. Perche F, Torchilin VP. Recent trends in multifunctional liposomal nanocarriers for enhanced tumor targeting. *J Drug Deliv.* 2013; 2013: 705265.
 38. Calle D, Cerdán S, Moreno F. Superparamagnetic Nanoparticles as a Contrast Agent for Magnetic Resonance Imaging (MRI) of Magnetic Susceptibility (T2*). 2013, PCT/ES2012/070044, WO 2013/110828.
 39. Torchilin VP, Weissig V. Liposomes: a practical approach. New York, USA: Oxford University Press; 2003.
 40. Floris A, Sinico C, Fadda AM, Lai F, Marongiu F, Scano A, et al. Characterization and cytotoxicity studies on liposome-hydrophobic magnetite hybrid colloids. *J Colloid Interface Sci.* 2014; 425: 118-27.
 41. Berne BJ. Dynamic light scattering: with applications to chemistry, biology and physics. Ontario, CAN: Dover Publications; 1976.
 42. Hallett FR, Watton J, Krygman P. Vesicle sizing: Number distributions by dynamic light scattering. *Biophys J.* 1991; 59: 357-62.
 43. Braun S, Kalinowski H-O, Berger S. 100 and more basic NMR experiments. VCH Weinheim; 1996.
 44. Rodríguez E, Roig A, Molins E, Arús C, Quintero MR, Cabañas ME, et al. In vitro characterization of an Fe8 cluster as potential MRI contrast agent. *NMR in Biomedicine.* 2005; 18: 300-7.
 45. Lee H, Lee K, Kim IK, Park TG. Synthesis, characterization, and in vivo diagnostic applications of hyaluronic acid immobilized gold nanoprobe. *Biomaterials.* 2008; 29: 4709-18.
 46. Camuesco D, Galvez J, Nieto A, Comalada M, Rodríguez-Cabezas ME, Concha A, et al. Dietary olive oil supplemented with fish oil, rich in EPA and DHA (n-3) polyunsaturated fatty acids, attenuates colonic inflammation in rats with DSS-induced colitis. *J Nutr.* 2005; 135: 687-94.
 47. Winking M, Sarikaya S, Rahmanian A, Jodicke A, Boker DK. Boswellic acids inhibit glioma growth: a new treatment option? *J Neurooncol.* 2000; 46: 97-103.
 48. Willker W, Leibfritz D. Assignment of mono- and polyunsaturated fatty acids in lipids of tissues and body fluids. *Magn Reson Chem.* 1998; 36: S84.
 49. Griffin JL, Lehtimäki KK, Valonen PK, Grohn OH, Kettunen MI, Ylä-Herttuala S, et al. Assignment of 1H nuclear magnetic resonance visible polyunsaturated fatty acids in BT4C gliomas undergoing ganciclovir-thymidine kinase gene therapy-induced programmed cell death. *Cancer Res.* 2003; 63: 3195-201.
 50. Bocian DF, Chan SI. NMR studies of membrane structure and dynamics. *Annu Rev Phys Chem.* 1978; 29: 307-35.
 51. Huber T, Rajamoorthi K, Kurze VF, Beyer K, Brown MF. Structure of docosahexaenoic acid-containing phospholipid bilayers as studied by (2)H NMR and molecular dynamics simulations. *J Am Chem Soc.* 2002; 124: 298-309.
 52. Valentine RC, Valentine DL. Omega-3 fatty acids in cellular membranes: a unified concept. *Prog Lipid Res.* 2004; 43: 383-402.
 53. Pelta MD, Barjat H, Morris GA, Davis AL, Hammond SJ. Pulse sequences for high-resolution diffusion-ordered spectroscopy (HR-DOSY). *Magn Reson Chem.* 1998; 36: 706-14.
 54. Einstein A. Über die von der molekularkinetischen Theorie der Wärme geforderte Bewegung von in ruhenden Flüssigkeiten suspendierten Teilchen. *Ann Phys-Berlin.* 1905; 322: 549-60.
 55. Cooper HS, Murthy SN, Shah RS, Sedergran DJ. Clinicopathologic study of dextran sulfate sodium experimental murine colitis. *Lab Invest.* 1993; 69: 238-49.
 56. Pacheco-Torres J, Calle D, Lizarbe B, Negri V, Ubide C, Fayos R, et al. Environmentally Sensitive Paramagnetic and Diamagnetic Contrast Agents for Nuclear Magnetic Resonance Imaging and Spectroscopy. *Curr Top Med Chem.* 2011; 11: 115-30.
 57. Merbach AE, Helm L, Tóth É. The Chemistry of Contrast Agents in Medical Magnetic Resonance Imaging. Chichester, UK: Wiley Online Library; 2013.
 58. Solomon I. Relaxation processes in a system of two spins. *Phys Rev.* 1955; 99: 559.
 59. Bloembergen N. Proton relaxation times in paramagnetic solutions. *J Chem Phys.* 1957; 27: 572.
 60. Bloembergen N, Morgan L. Proton relaxation times in paramagnetic solutions. Effects of electron spin relaxation. *J Chem Phys.* 1961; 34: 842.
 61. Skouras A, Mourtas S, Markoutsas E, De Goltstein MC, Wallon C, Catoen S, et al. Magnetoliposomes with high USPIO entrapping efficiency, stability and magnetic properties. *Nanomedicine.* 2011; 7: 572-9.
 62. Garnier B, Tan S, Miraux S, Bled E, Brisson AR. Optimized synthesis of 100 nm diameter magnetoliposomes with high content of maghemite particles and high MRI effect. *Contrast Media Mol Imaging.* 2012; 7: 231-9.
 63. Carvalho A, Goncalves MC, Martins MB, Meixedo D, Feio G. Relaxivities of magnetoliposomes: the effect of cholesterol. *Magn Reson Imaging.* 2013; 31: 610-2.
 64. Jensi LJ, Zerouga M, Stillwell W. Omega-3 fatty acid-containing liposomes in cancer therapy. *Proc Soc Exp Biol Med.* 1995; 210: 227-33.
 65. Schrooyen PM, van der Meer R, De Kruif CG. Microencapsulation: its application in nutrition. *Proc Nutr Soc.* 2001; 60: 475-9.
 66. Holser R. Encapsulation of Polyunsaturated Fatty Acid Esters with Solid Lipid Particles. *Lipid Insights.* 2011; 5: 1-5.
 67. Fearon K, Ljungqvist O, Von Meyenfeldt M, Revhaug A, Dejong C, Lassen K, et al. Enhanced recovery after surgery: a consensus review of clinical care for patients undergoing colonic resection. *Clin Nutr.* 2005; 24: 466-77.
 68. Dixon SJ, Stockwell BR. The role of iron and reactive oxygen species in cell death. *Nat Chem Biol.* 2014; 10: 9-17.
 69. Calle D, Cerdán S, Moreno F. Liposomal formulations containing omega-3 poly-unsaturated long chain fatty acids and superparamagnetic nanoparticles and their therapeutic use in malign tumors 2014, P201430035.

Author Biographies



Daniel Calle obtained his PhD in from the Autonomous University of Madrid in novel nanotechnological formulations detectable in vivo by multimodal imaging methods as MRI, PET/SPECT/CT or Fluorescence/ Bioluminescence. He has coauthored four publications and holds three patents. His current research interests include; 1) Development of novel strategies for image guided drug delivery and 2) Development of advanced anti-inflammatory formulations.



Viviana Negri obtained her Bs in Chemistry from the University of Milano (IT) and her Master Degree in Organic Chemistry from the Complutense University of Madrid (ES). She is coauthor of eight publications and holds two patents. Her research interests include: 1) Development of novel MRI contrast agents based in graphene structures and 2) Characterization of Nanotechnological formulations using advanced Magnetic Resonance Spectroscopy methods.



Paloma Ballesteros is Professor of Organic Chemistry and Molecular Imaging at the National University of Education at a Distance in Madrid (ES). She has coauthored more than ninety publications including *Angew. Chem. Int. Ed.*, *J. Org. Chem.* and *Organic Syntheses* and holds five patents. Her current interests include: 1) Development of efficient theranostic formulations against cancer, obesity and inflammation, 2) Development of decorated graphene structures observable by MRI and 3) Implementation of new methods to detect molecular anisotropy and 3D orientation in vivo by MRI.



Sebastián Cerdán is Professor of Biomedical Imaging at the Higher Council of Scientific Research in Madrid (ES). He has coauthored over 150 publications including *Nature Comm.*, *Angew. Chemie Int. Ed.*, *Proc. Natl. Acad. Sci. (USA)* and *Neuroimage*. He holds five patents. His current research interests include: 1) Non-invasive detection of inflammation and anti-inflammatory effects, 2) Development of multimodal imaging contrast agents; and 3) Operator-free intelligent image interpretation.